CSIRO PUBLISHING

International Journal of Wildland Fire **2014**, *23*, 755–770
http://dx.doi.org/10.1071/WF12194

Simulation and thermal imaging of the 2006 Esperanza Wildfire in southern California: application of a coupled weather–wildland fire model

Janice L. Coen[A,C] *and Philip J. Riggan*[B]

[A]National Center for Atmospheric Research, PO Box 3000, Boulder, CO 80307-3000, USA.
[B]Pacific Southwest Research Station, USDA Forest Service, 4955 Canyon Crest Drive, Riverside, CA 92507, USA.
[C]Corresponding author. Email: janicec@ucar.edu

Abstract. The 2006 Esperanza Fire in Riverside County, California, was simulated with the Coupled Atmosphere–Wildland Fire Environment (CAWFE) model to examine how dynamic interactions of the atmosphere with large-scale fire spread and energy release may affect observed patterns of fire behaviour as mapped using the FireMapper thermal-imaging radiometer. CAWFE simulated the meteorological flow in and near the fire, the fire's growth as influenced by gusty Santa Ana winds and interactions between the fire and weather through fire-induced winds during the first day of burning. The airflow was characterised by thermally stratified, two-layer flow channelled between the San Bernardino and San Jacinto mountain ranges with transient flow accelerations driving the fire in Cabazon Peak's lee. The simulation reproduced distinguishing features of the fire including its overall direction and width, rapid spread west-south-westward across canyons, spread up canyons crossing its southern flank, splitting into two heading regions and feathering of the fire line. The simulation correctly depicted the fire's location at the time of an early-morning incident involving firefighter fatalities. It also depicted periods of deep plume growth, but anomalously described downhill spread of the head of the fire under weak winds that was less rapid than observed. Although capturing the meteorological flow was essential to reproducing the fire's evolution, fuel factors including fuel load appeared to play a secondary role.

Additional keywords: airborne remote sensing, coupled atmosphere–fire model, fire behaviour, horizontal roll vortices, Santa Ana winds.

Received 19 November 2012, accepted 7 April 2014, published online 9 July 2014

Introduction

Our ability to learn from previous wildland fire events is limited by our understanding about how factors such as evolving weather, fuels and terrain combine; and why. Operational models such as BehavePlus (Andrews 2009) and FARSITE (Finney 1998) are used by US land management agencies to predict the movement of wildland fires across landscapes. These 'kinematic' models consider weather, terrain and fuels as largely external, non-interacting variables and do not explicitly represent the forces involved in fire propagation. In contrast, coupled weather–wildland fire models, which interactively join a description of fire behaviour with a full numerical weather prediction model, simulate not only the direction and rate of fire propagation but also the dynamic forces that determine a fire's evolution, including its alteration of the flow and structure of the atmosphere by the release of heat and moisture.

Here we present the application of one such interactive model, the Coupled Atmosphere–Wildland Fire Environment (CAWFE) model, to the simulation of the 2006 Esperanza Fire, which was ignited near Cabazon, California, and swept through chaparral, coastal sagebrush and annual grasses along the northern flank of the San Jacinto Mountains during a moderate Santa Ana wind event. We describe the atmospheric regime in which the fire occurred, summarise salient characteristics of the simulation, analyse the sensitivity of the simulation to fuel and modelling parameters, and compare some simulated and observed fire properties. This work represents a test or partial validation of the model under complex, actual conditions.

Background

Santa Ana wind events occur when a high-pressure system over the Great Basin drives air south-westward across the Transverse and Peninsular ranges of southern California towards low pressure offshore. Events are typically associated with strong, gusty winds and very low relative humidity. Air crossing the mountain ranges is channelled and accelerated through passes and canyons, notably in the Santa Clara River Valley, along the

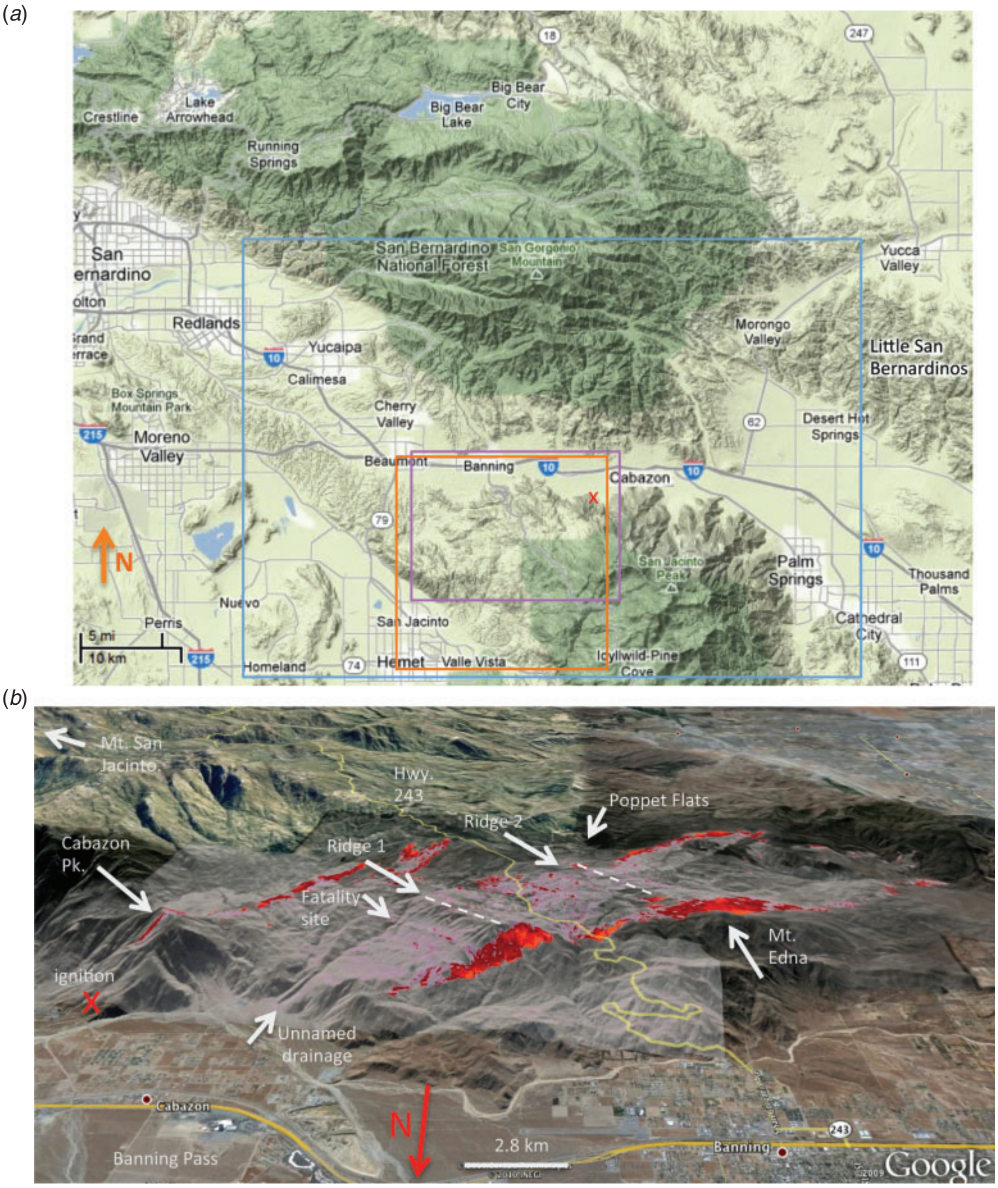

Fig. 1. (*a*) Map of local area, with outlines of model Domains 4 and 5 and the area covered by Fig. 1*b* respectively outlined in blue, magenta and orange. (*b*) Incident locations and topographic features over which the 1117 hours Pacific Daylight Time FireMapper imagery are shown. The red 'X' indicates ignition location.

Santa Ana River canyon between Riverside and Orange counties, below the Santa Suzanna and Cajon passes, and along Banning Pass between the San Bernardino and San Jacinto mountains (Whiteman 2000). Santa Ana events are common from September through April and create the greatest fire risk when they coincide with low live fuel moisture during late summer and autumn (Schroeder *et al.* 1964; Dennison *et al.* 2008). Although a strong offshore pressure gradient is indicative of Santa Ana conditions, the strength of surface winds may be comparably influenced by synoptic forcing such as downward momentum transfer from a strong upper-level offshore flow and by smaller-scale factors such as near-surface flow that is forced by a strong temperature gradient from the high desert to the ocean and modified by flow through complex terrain (Hughes and Hall 2010). Only a few studies have examined Santa Ana flow dynamics, such as the breaking of gravity waves, surfacing of strong upper-level winds (Huang *et al.* 2009) and channelling of winds around barriers and through passes and canyons (Fosberg 1965; Fosberg *et al.* 1966; Ryan 1969).

Following its ignition at 0112 hours Pacific Daylight Time (PDT) on 26 October 2006, the Esperanza Fire initially spread up steep slopes on Cabazon Peak and hence west-south-westward (Fig. 1*a*), burning 9700 ha in 18 h. By 0730 hours PDT the fire had overrun a firefighting crew west of Cabazon Peak that was defending a home at the top of a minor, unnamed topographic drainage, causing five fatalities. A subsequent investigation of that incident described fire suppression operations, fuels, weather and fire behaviour (Esperanza Investigation Team 2007). By containment on 30 October 2006, the fire had burned ~16 300 ha (40 200 acres).

Model description

CAWFE couples a three-dimensional, non-hydrostatic numerical weather prediction model with a fire behaviour module that describes the propagation of a wildland fire in response to spatially varying terrain and fuels, and spatially and temporally evolving weather. The modelling system can represent the complex interactions between a fire and the atmosphere: low-level winds drive spread of the fire, which releases sensible heat, latent heat and smoke into the lower atmosphere at rates that vary in space and time according to the rate at which fuel is consumed. The heat fluxes, in turn, feed back to affect the winds directing the fire.

Fire module components treat physical processes including the flaming front's rate of spread, post-frontal heat release, crown fire ignition and consumption, and up-scaling of heat release into the atmospheric model. An additional algorithm defines the subgrid-scale interface between burning and un-ignited fuel. Because it is designed to resolve atmospheric motions from tens of metres to hundreds of kilometres, and combustion processes occur at scales several orders of magnitude smaller than that, CAWFE does not explicitly simulate flames or combustion; neither the fuel or fire temperature, nor the consumption of oxygen or flammable pyrolysed gases are tracked by this model. Instead, CAWFE parameterises these subgrid-scale processes by adapting semi-empirical and empirical relationships. Coen (2013) described a recent version of CAWFE; subsequent development is described below. Coen and Schroeder (2013) applied CAWFE using new satellite remote sensing active fire-detection data to introduce a wildfire already in progress into the model and to evaluate the simulated growth at later times.

Riggan *et al.* (1994) noted that in the absence of substantial deadwood biomass, fire spreads through natural chaparral stands only with low live fuel moisture and either wind or steep terrain. Weise *et al.* (2005) developed and tested a model to predict the probability of fire spread in living fuels in marginal burning conditions. However, a threshold wind speed for such sustained spread has not been determined, and indeed, there have been only limited measurements of the rate of fire spread through chaparral, that is, during prescribed burning under low wind velocity (Stephens *et al.* 2008). This threshold behaviour suggests that the mechanism for spread is piloted ignition of nearby shrubs by flame contact. Cheney *et al.* (1998) noted that sustained spread of a heading fire through pastures required a wind velocity greater than 1.4 m s^{-1} at 10 m above ground level (AGL). We have incorporated this contact ignition perspective into our rate of spread calculation and, until research reveals what this threshold should be in other fuel types, apply a non-zero wind coefficient (as defined by Rothermel 1972) only at wind speeds greater than 0.55 m s^{-1}, which is Cheney *et al.*'s threshold adjusted by a logarithmic profile typical of atmospheric surface layers to the 2 m height typical of chaparral fuels.

Airborne remote sensing of the Esperanza incident

The Pacific Southwest Research Station of the US Department of Agriculture (USDA) Forest Service applied its airborne FireMapper thermal-imaging radiometer during the Esperanza Fire to obtain unprecedented, high-resolution measurements of the behaviour across an entire wildland fire under the influence of Santa Ana winds. The FireMapper employs a BAE Systems (Lexington, MA) microbolometer focal plane array and two levels of onboard calibration to measure and map upwelling thermal radiation in a broad band channel encompassing wavelengths from 8 to 12.5 μm and narrow band channels at 8.1–9.0 and 11.5–12.3 μm. The latter narrow band channel provides unsaturated data over large wildland fires. Quantitative image data from individual aircraft passes on 26 October were assembled into six orthorectified maps that depicted the fire's progress and apparent spread rate between 1117 and 2142 hours PDT. Radiometric temperature and radiant flux density measurements at long-wave infrared wavelengths primarily are indicative of ground surface temperatures, even beneath active fire fronts, and thereby indicate radiant fire intensity, local variations in fire energy release and flaming front depth and residence time.

Model initialisation and experimental design

Atmospheric model initialisation

A Weather Research and Forecasting (WRF) model regional weather simulation with two nested domains (with 30- and 10-km horizontal grid spacing) was initialised with data from the National Center for Environmental Prediction's final Operational Global Analysis and applied to simulate the period 1200 UTC 25 October 2006 (0500 hours PDT) to 1200 UTC 27 October 2006. The WRF simulation provided initial conditions and boundary conditions for the finer resolution CAWFE model simulation (Fig. 1*b*). Terrain for the modelling domains was derived from 0.33-, 1- and 3-arc-second elevation data. Near the fire, the terrain is dominated by Mount San Jacinto (elevation 3302 m) and Mount San Gorgonio (elevation 3506 m), which are separated by the west–east oriented Banning Pass with a maximum elevation of 485 m (Fig. 1*a*).

Fuel characteristics and condition

The spatial distribution of fuel properties in CAWFE's innermost modelling domain (Fig. 2) was obtained from the LANDFIRE geospatial database (see http://www.landfire.gov, accessed 19 December 2011), which was developed from satellite remote sensing data and limited *in-situ* sampling. LANDFIRE classifies fuels into stylised fuel models using the Albini (1976) classification system as restated by Anderson (1982). Low terrain at Banning Pass, greater Cabazon and the ignition point were classified as un-vegetated or covered by short grass; either Fuel Model 4 (mature chaparral) or Fuel Model 5 (young chaparral with little dead fuel) characterised vegetation on mid-level slopes. Fuel properties are given in Table 1. Given that fire spread in chaparral often coincides with low live fuel moisture (Riggan *et al.* 1994; Dennison *et al.* 2008), it is possible that fire spread in such fuels is influenced by live fuel moisture; however, experimental studies in shrubs

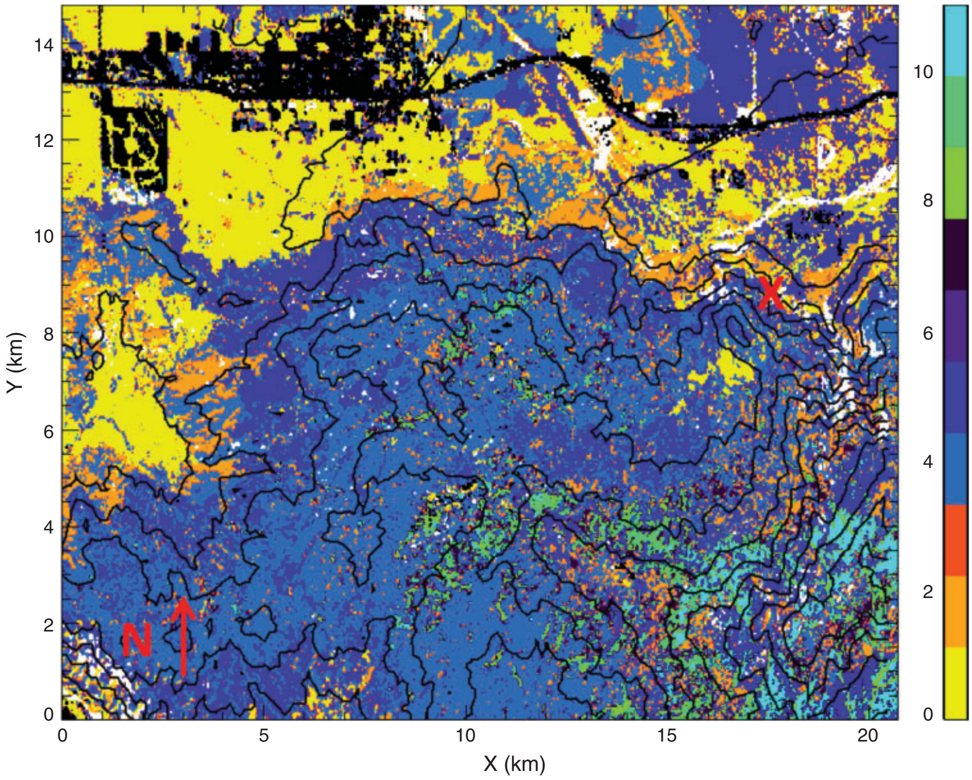

Fig. 2. Spatial distribution of fuel models in the innermost modelling domain (Domain 5), categorised by the Anderson (1982) fuel model classification system. Fuel models are given by colour bar at right, where white indicates no fuel. The terrain contour interval is 150 m. Fuel model properties are given in Table 1. The red 'X' indicates the ignition location.

Table 1. Fuel models used in the innermost modelling domain
Columns show fuel properties associated with each fuel model

Fuel model	Name	Surface fuel load (kg m^{-2})	Weighting parameter, W (s)	Surface area to volume ratio, σ (m^{-1})	Fuel depth (m)	Fuel moisture content of extinction	Canopy fuel load (kg m^{-2})	Canopy fuel burnout time (s)
1	Short grass	0.167	7	11 483	0.305	0.12	0	–
2	Grass + understorey	0.896	30	7500	0.610	0.15	0	–
4	Chaparral	3.591	360	4400	2.000	0.20	0	–
5	Brush	0.784	360	5100	0.667	0.20	0	–
7	Southern rough	1.091	360	5125	0.762	0.40	0	–
8	Closed timber litter	1.120	1200	2089	0.061	0.30	1.121	60
9	Hardwood litter	0.780	1200	6916	0.061	0.25	1.121	120
10	Timber litter + understorey	2.692	1200	2089	0.305	0.25	1.121	180
99	No vegetation	0.000	–	–	–	–	–	–

(Fernandes *et al.* 2000; Fernandes 2001; Bilgili and Saglam 2003) have not found live moisture content to have a significant effect on rate of spread, other than a weak connection in oak chaparral (Lindenmuth and Davis 1973). This influence could manifest in several ways, by affecting (1) a probability of spread in marginal conditions (Weise *et al.* 2005), (2) a threshold wind speed below which fire will not spread or (3) the rate of spread itself. We acknowledge that live fuel moisture may affect rate of spread, but have not included it in our formulation because there is no evidence that distinguishes if or how live fuel moisture affects the rate of spread in chaparral or similar fuels, and schemes for describing the live fuel moisture effect on rate of spread in chaparral (e.g. Fosberg and Schroeder 1973) either are largely untested or could not be applied: in one situation they produced a composite fuel moisture above the moisture content of extinction. Consequently, we set fuel moisture for all fuel models to 6% based on diagnosed 10-h dead fuel moisture at nearby remote automated weather stations (RAWS). This

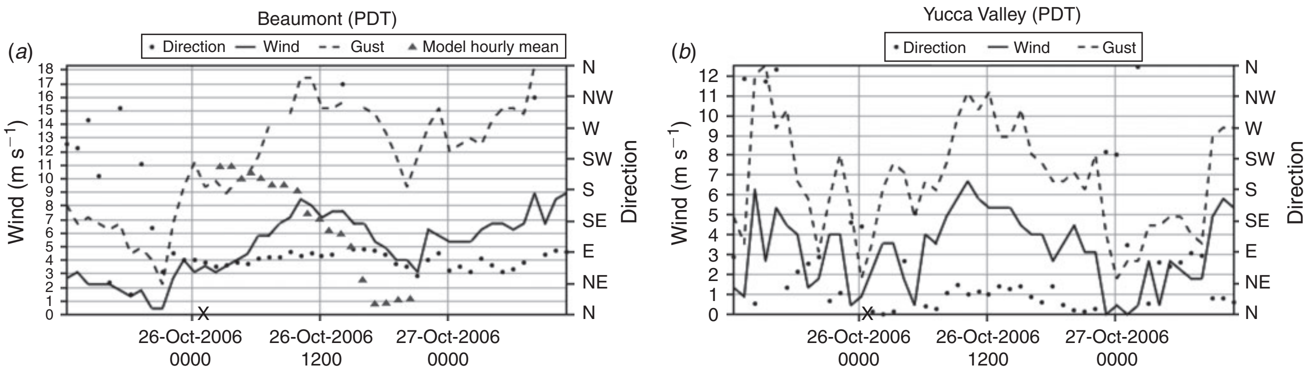

Fig. 3. RAWS surface weather station data from MesoWest for the period 1200 hours Pacific Daylight Time 25 October 2006 – 1200 hours 27 October 2006 at (*a*) Beaumont, with model Domain 5's hourly mean wind speed interpolated to 6.1 m above ground level and (*b*) Yucca Valley. The 'X' on the x-axis indicates ignition time.

approach is in accordance with our hypothesis that fire propagation in grasses and shrubs occurs through piloted ignition of fine, dead fuel.

Experimental design

Beginning with the atmospheric state given by the WRF simulation at 2200 UTC 25 October 2006 (1500 hours PDT), CAWFE first simulated 10 h of weather before the fire's ignition. During this time, CAWFE refined the horizontal grid spacing from 10.0 km in its coarsest modelling domain (a $980 \times 980 \times 15.6$-km domain covering the western USA) to 3.33 km, 1.11 km, 0.370 km and 0.123 km in the finest resolution modelling domain (a $21.0 \times 14.8 \times 6.2$-km domain covering Banning Pass and the San Jacinto Mountains) in which fire growth is modelled. The stretched vertical grid was correspondingly refined. The finest domain's first three grid levels were located at 16, 36 and 62 m, with the first half-grid level (where the lowest horizontal wind components are located) at 7.9 m above ground. Shear forces drove the turbulent boundary layer's development; solar heating of the surface was not considered. The atmospheric wind was dominated by the synoptic-scale weather modified by motion over and around topographic features, in addition to stresses produced by topographic gradients and surface stresses that arose from vegetation roughness. At the reported ignition time, the simulation ignited a fire in the finest domain above the wash on the north-east side of Cabazon Peak. The model simulated the subsequent 19 h of weather and fire behaviour.

A second experiment repeated the simulation without igniting a fire. Examining the mathematical difference between these two simulations showed to what extent the fire altered the atmospheric environment. Other sensitivity experiments varied parameters used in applying the fire's feedback to the atmosphere and tested the sensitivity of CAWFE to fuel parameters because these may affect simulations in a dynamic model differently than kinematic models such as FARSITE.

Results

Simulated atmospheric flow and Santa Ana structure

During this 2.5-day Santa Ana event, recorded wind speeds at nearby Beaumont (Fig. 3*a*) and Yucca Valley (Fig. 3*b*), California, peaked at 1100 hours PDT on the fire's first day and changed slowly in direction as the high-pressure centre over the Great Basin moved east. The simulated Santa Ana winds at Beaumont (Fig. 3*a*) were stronger at the initiation of Domain 5 than were the RAWS data and weakened earlier than observed. The CAWFE simulation showed that, as is typical during such events, winds rotated counter-clockwise with increasing height throughout the troposphere, as low-level winds from the north-east turned counter clockwise with increasing height, coming from the south-west at the tropopause (13 km). The simulation also showed that the lower atmosphere's vertical structure was composed of two layers – a 500 m-deep layer near the surface that was highly stable to vertical motions (with Brunt–Vaisala frequency $n = 0.022\ \mathrm{s}^{-1}$, equivalent to a lapse rate of $5.0\ \mathrm{K\ km}^{-1}$) with strong orographically enhanced winds that peaked at 300 m AGL. Over this lay a moderately stable layer (with $n = 0.011\ \mathrm{s}^{-1}$, a lapse rate of $6.4\ \mathrm{K\ km}^{-1}$) that extended up to 9.5 km above mean sea level (MSL) with weaker winds from 2–6 km AGL. This vertical wind shear, in combination with the stable, layered atmospheric structure, made possible a range of complex orographic atmospheric flow regimes, particularly considering the dramatic and varied terrain in the study region.

During the Santa Ana, strongly stably stratified winds entered the region from the north-east, were blocked by Mount San Gorgonio, and were channelled down the Yucca and Morongo Valleys between Mount San Gorgonio and the Little San Bernardino Mountains (1200–1740-m elevation) and, to some extent, over the Little San Bernardino Mountains (Fig. 4). Flow over the mountains excited in their lee trapped gravity waves, which are an oscillation arising from the fluid's vertical temperature gradients. Shear-generated turbulence and wave motions triggered by the Little San Bernardino Mountains also contributed to transience in the winds that affected the fire downstream. Exiting the Morongo Valley, the strongly stably stratified, low-level winds were blocked by the 3000 m face of Mount San Jacinto, which split the flow eastward down into Palm Springs in the Coachella Valley and westward, where it was accelerated by the effects of Bernoulli's principle (Batchelor 1967) as it was channelled up into the narrow, steep-walled Banning Pass.

Idealised studies of a similar flow regime, in which stable airflows of low Froude number encounter mountains, have been

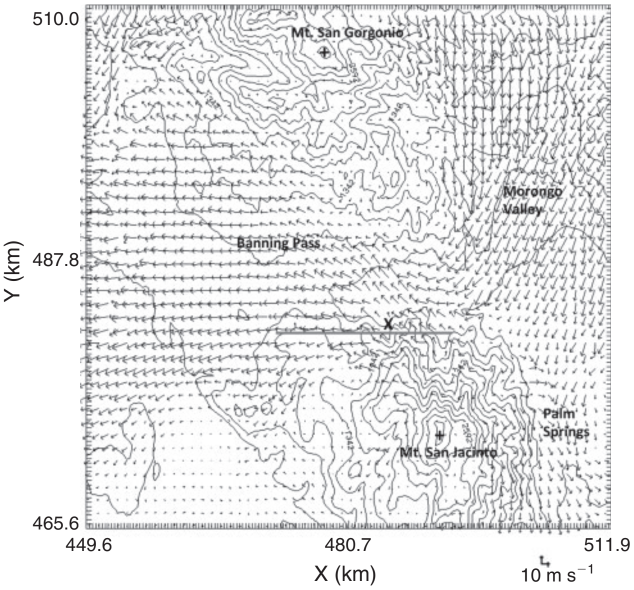

Fig. 4. Modelled wind speeds in Domain 4 at 7.9 m above ground level at 0045 hours Pacific Daylight Time on 26 October 2006. Topography contours are shown every 250 m. The grey line indicates the location of the cross section in Fig. 5.

described by Hunt *et al.* (1997). The Froude number is given by $Fr = U(nh)^{-1}$, where U is the ambient air speed (m s^{-1}), n is the Brunt–Vaisala frequency (s^{-1}) and h (m) is the mountain height. Weakly stratified flows ($Fr > 1$) around three-dimensional objects are generally well understood, particularly when the terrain slope is small. Stably stratified flows are more complex and often involve nonlinear effects (e.g. Vosper *et al.* 1999). In these simulations, with higher velocity airflow than in Hunt *et al.* (1997), air impinging on Mount San Jacinto rode upslope above its level of neutral buoyancy. Becoming cooler than its surroundings, it spilled down the lower slopes of Mount San Jacinto north-westward, producing gusts each 5–7 min. A theoretical basis for this frequency is not available because of the complex environment. As air descended, some of it crossed Cabazon Peak (1382 m above MSL). The combined thermal stratification (Fig. 5*a*) and wind structure (Fig. 5*b*) of this flow over Cabazon Peak, where we estimated Fr to be 1.1 at mountaintop, caused the flow to become supercritical, as in Durran's (1986) idealised two-layer two-dimensional flow simulations in this Froude number regime. This caused a sharp increase in descending lee-side, near-surface winds that resembled a hydraulic jump, although that analogy is not exact (Durran 1986). This combination created dramatic unsteady topographic flow accelerations (not shown) down into the lower section of an unnamed drainage west of Cabazon Peak in which the fire established itself. A photograph (Fig. 6) taken from north-west of the smoke plume during this period documents the fast-moving stable layer of air trapped near the ground and the wind's hydraulic jump-like structure. Thus, in contrast to conclusions based on the perceived alignment of the prevailing Santa Ana flow with the unnamed drainage, the simulation indicated that airflow was not channelled up into the south-west-to-north-east-oriented, unnamed drainage from Banning Pass. Not until the air reached less steep walls further downwind did the near-surface winds channelled through Banning Pass fan out onto the upland south of the pass. Some upland areas were sheltered from the Santa Ana winds by topographic features including the topographic bowl south of Cabazon Peak containing the Twin Pines Ranch and the area south-west of two north-west-to-south-east trending ridges straddling State Route 243 that ultimately bisected the fire.

The coupled weather–fire simulations were sensitive to the amount of diffusion, a combination of natural atmospheric mixing and necessary numerical smoothing, which reduced strong gradients in the atmospheric state. Simulations with less mixing built strong potential temperature and velocity gradients that led to gravity wave overturning and breaking over Cabazon Peak. Experiments with strong mixing, in the form of background numerical dissipation, numerical filters, or coarser vertical resolution, experienced strong winds only in Banning Pass. In those trials, strong winds and the simulated fire did not extend up to the slopes that burned and, although acceleration occurred over Cabazon Peak, the airflow had weaker mountaintop winds and did not produce dramatic flow amplification in its lee.

As is common in mountainous areas, limited verification data were available even for near-surface wind fields. Only the Beaumont RAWS was located in the area covered by the simulation's innermost domain; that station reported only 10-min average wind speed and gusts over the previous 1 h, which was insufficient to evaluate the gust frequency produced in the model.

Modelled fire growth and behaviour

The Esperanza Fire event was a complex, shifting interplay between (1) advances driven by the local, time-varying wind, (2) local topographic effects on the fire that included not only the inclination of a flat surface but also the concavity of canyons, (3) occasions for particularly enhanced growth when wind and topographic effects compounded each other, and (4) occasions when they opposed each other.

Following ignition, the simulated fire traversed Cabazon Peak's north face and, while experiencing strong winds in the supercritical flow in its lee or west side (as discussed in the previous section), was rapidly driven down into the unnamed drainage's base (in agreement with Esperanza Investigation Team 2007) with rates of spread ranging from 0.2 to 1.6 m s^{-1} (Fig. 7*a*).

From 0450 to 0620 hours PDT, the spear-shaped fire's leading edge spread downwind (west-south-westward) primarily across, rather than up, the unnamed drainage, with enhanced growth on its southern, upslope flank where it lay in the drainage (Fig. 7*b*). The momentum created by this heat release in the drainage was transported downwind to the head, further accelerating the head downwind.

As it ascended from the drainage, the fire front became uneven, developing multiple lobes that extended forward along the front (Fig. 7*b*), as locations along the fireline encountered upward-leading canyons, air currents, or possibly fuel properties favouring faster growth. The fire front developed protuberances along the heading region and flanks that were drawn up drainages that it crossed. One of these grew from the north

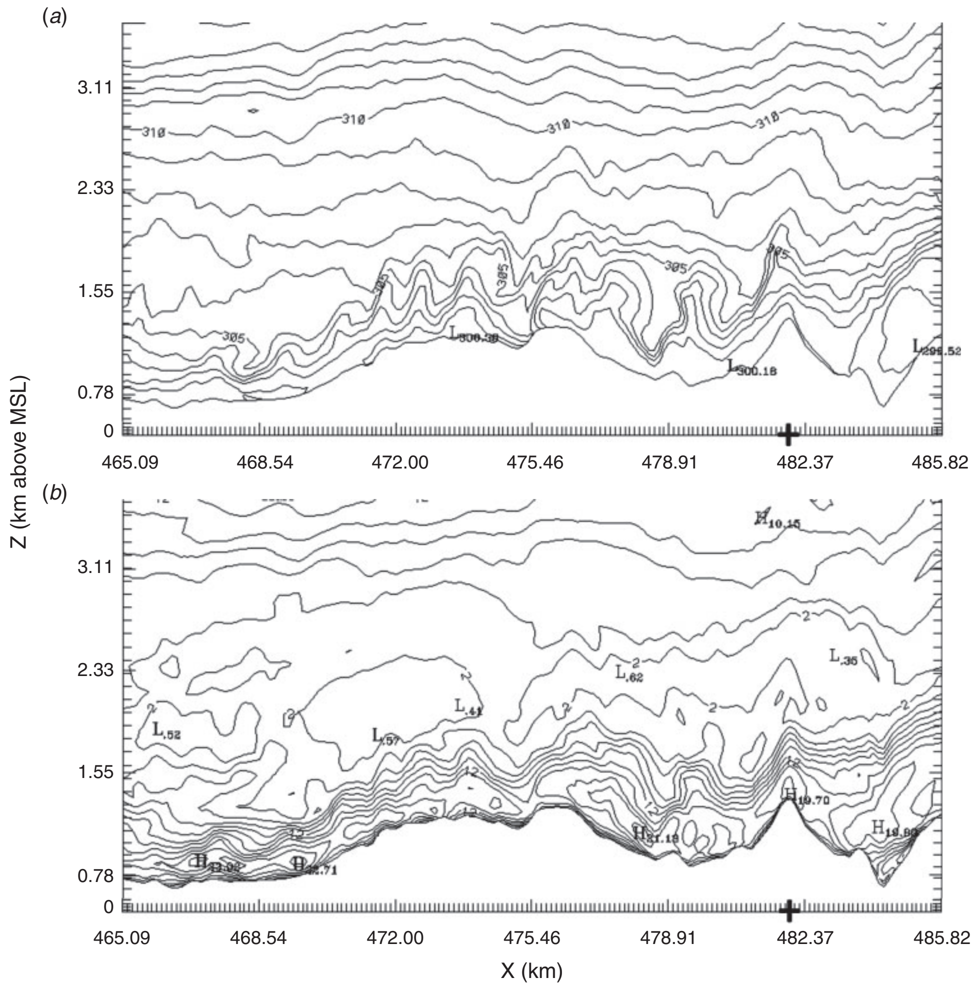

Fig. 5. Vertical west–east cross section (location shown in Fig. 4) through Cabazon Peak (indicated by '+' on the *x*-axis) of (*a*) potential temperature (contour every 1 K) and (*b*) wind speed (contour every 2 m s^{-1}) at 0045 hours Pacific Daylight Time. The wind indicated in this image was travelling from right to left, opposite to Fig. 6. MSL, mean sea level.

Fig. 6. The wind is travelling left to right in this image, taken at ~0800 hours Pacific Daylight Time. The smoke plume outlines the fast-moving stable layer of winds trapped near the ground and the hydraulic jump-like structure of the winds during the first morning of the fire. Photo courtesy of Jeff Zimmerman.

flank and became a flank run (Fig. 7*c*). The southern (upslope) flank, along which winds blew parallel and slightly into the fire, climbed upslope all along its length. For the 10-h period from ignition until the research aircraft's arrival, few data for validation exist other than the location and approximate time of the engine crew entrapment (Esperanza Investigation Team 2007). At that time in the simulation, the upslope flank of the southern heading region lay only 0.13 km past the entrapment site (Fig. 7*c*), with a 1 km-wide vertically oriented vortex located overhead. The simulation suggested that the heading region had

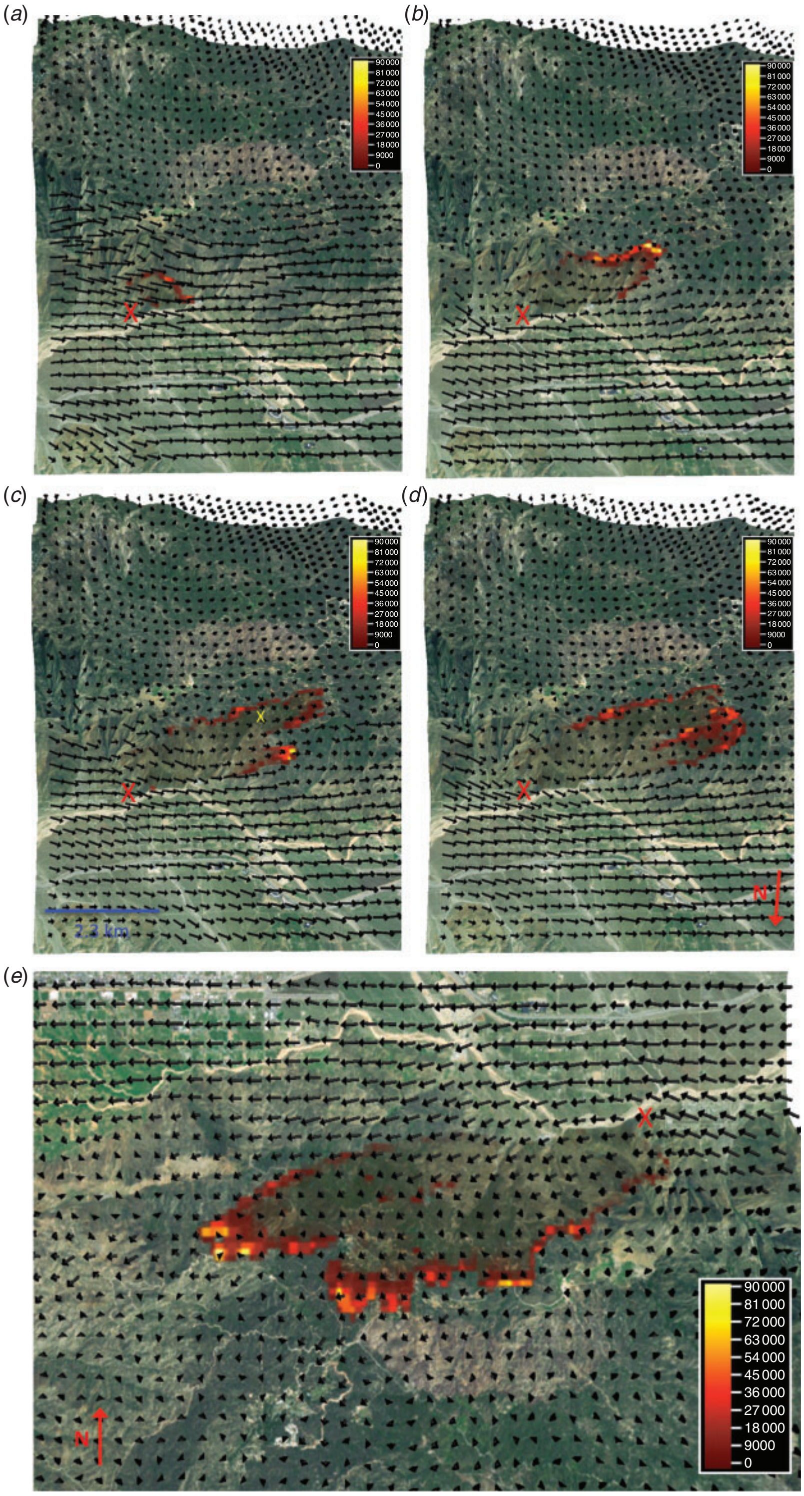

Fig. 7. Modelled fire heat flux (given by colour bar), and vectors showing the wind every third model grid cell, are shown at 20 m above ground level at (*a*) 0255 hours, (*b*) 0554 hours, (*c*) 0718 hours (where the yellow 'X' indicates the fatality location), (*d*) 0815 hours and (*e*) 1012 hours Pacific Daylight Time. The red 'X' indicates the ignition location.

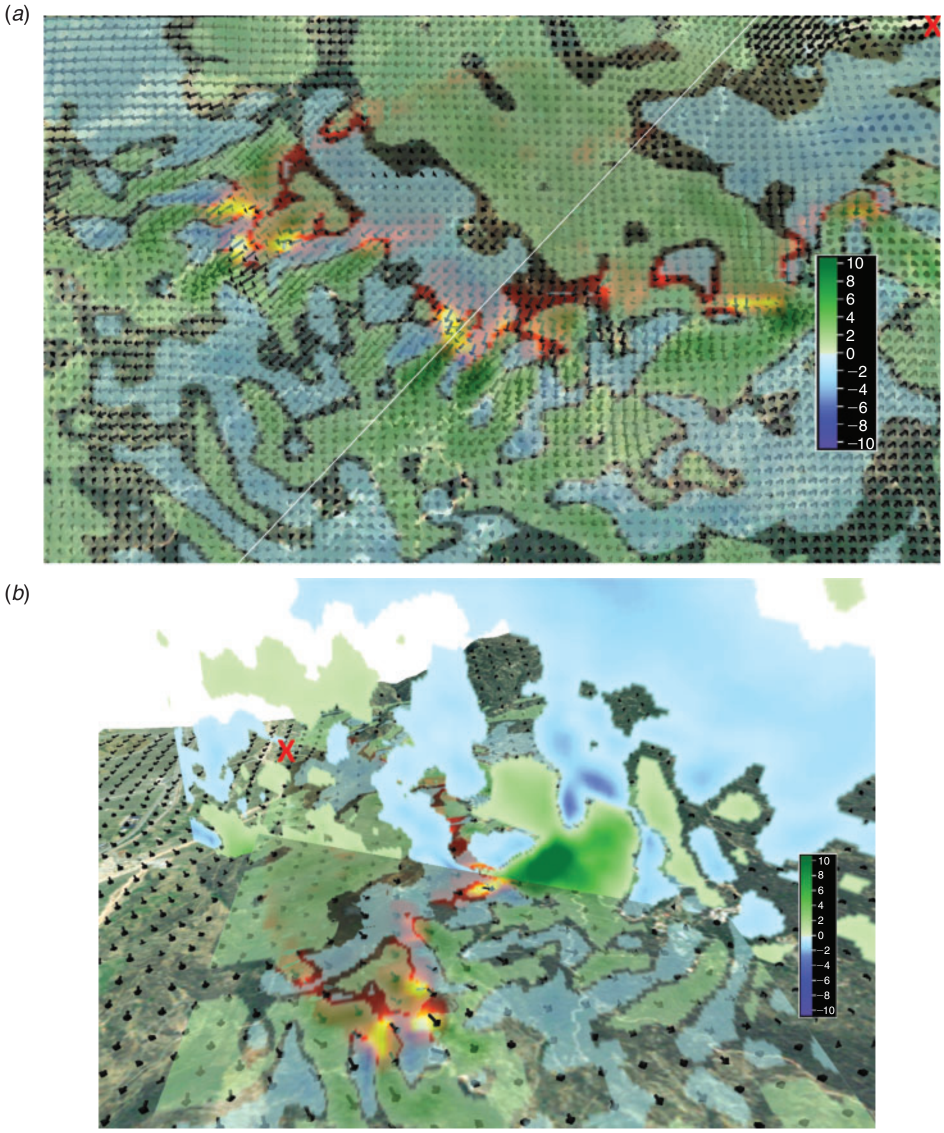

Fig. 8. Cross sections at 1012 hours Pacific Daylight Time, the same time as Fig. 7*e*, of vertical velocity (given by the colour bar, where positive is upward motion in m s^{-1} and values from −0.75 to 0.75 m s^{-1} are transparent) in (*a*) a near-surface plane where the southern edge is inclined 2° above horizontal and (*b*) a vertical plane (the location is shown as a white line in (*a*)) through the southern heading region at an angle 33° clockwise from north. The red 'X' indicates the ignition location.

passed downwind across the unnamed drainage and its upslope flank was climbing through this location, with faster rates of spread through topographic chimneys.

The fire's two heading regions subsequently rejoined (Fig. 7*d*), leaving pockets of unburned fuel between them, before splitting again (Fig. 7*e*). This occurred because the northern head was driven downwind west-south-westward across canyons by ambient winds aided by smooth, upwardly inclined terrain. The fire's southern head simultaneously travelled south-west, its head and upslope southern flank drawn up topographic chimneys, while east-south-easterly winds, blowing along and slightly into the fire perimeter, widened the head to the west by encouraging lateral wind-driven growth on the downwind side. Each of these two major heading regions developed multiple fingers along their leading edges as locally favourable growth paths, such as upward-tilted draws, encouraged locally faster spread.

Cross sections approximately tangent to the surface (Fig. 8*a*) and vertically through the southern head of the modelled fire (Fig. 8*b*) revealed the wind structure in the fire's vicinity. Updrafts several hundreds of metres wide with maximum vertical velocities of 10–20 m s^{-1} lay along the fire front and leaned downwind ahead of the fire line. Under these inclined updrafts there was confluence in surface winds. In between the updrafts lay 5–10 m s^{-1} downdrafts, under which there was diffluence in surface winds. This pattern indicates a row of

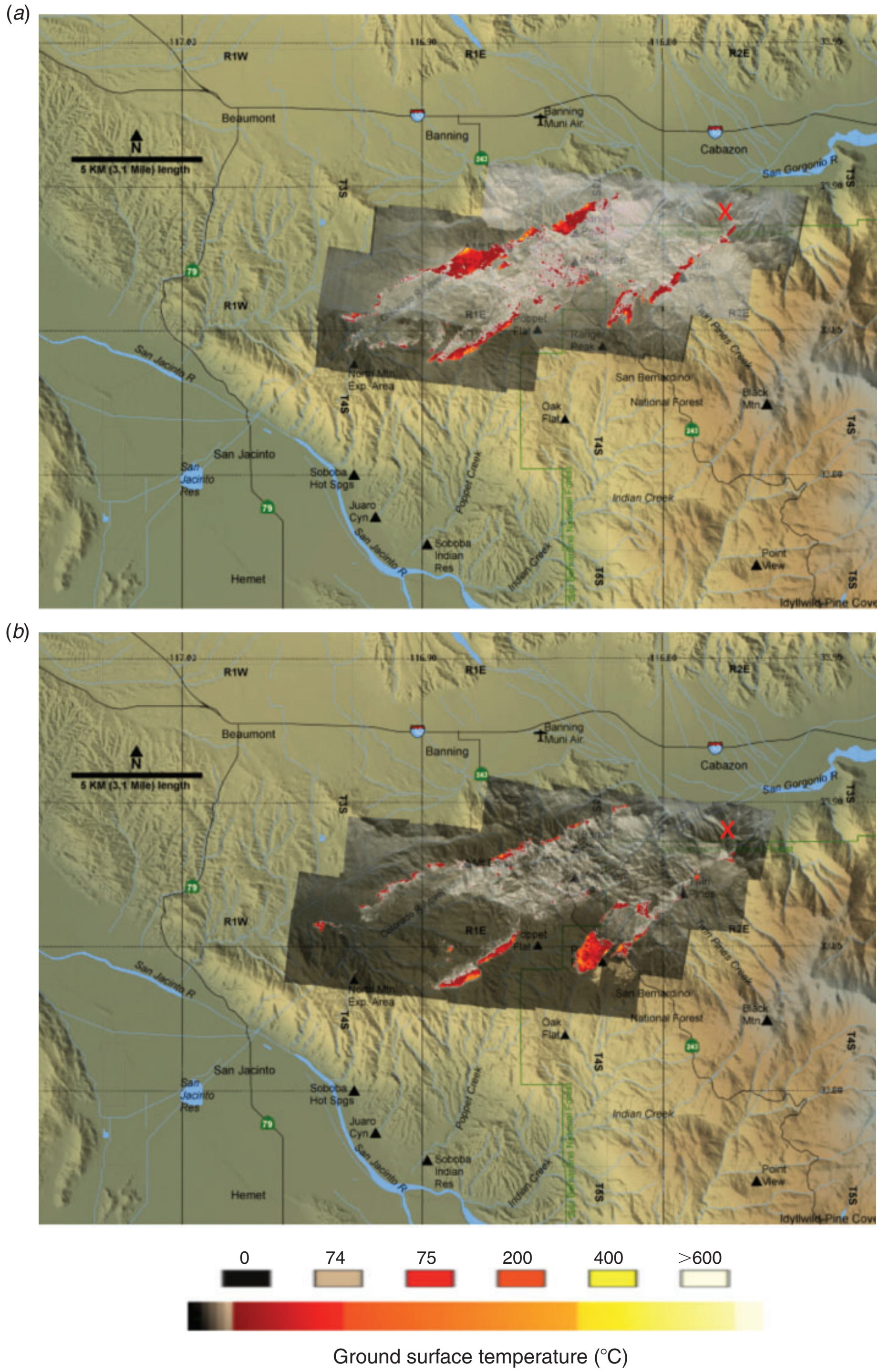

Fig. 9. Ground surface temperature derived from FireMapper long-wave data at (*a*) 1117 hours and (*b*) 1302 hours Pacific Daylight Time. The red 'X' indicates ignition location.

inclined horizontal roll vortices, described in crown fires by Haines (1982). A swathe of air descending at 2–5 m s^{-1} behind the fire line (Fig. 8*b*) supplied air into the inclined rotating plumes. The locally steeper terrain on the sides of the notched drainage was seen to increase fire rate of spread, the rate of heat release, updraft strength and confluence of winds into the plume base, and thereby further increase the rate of spread. Thus, whereas upwardly sloped terrain increases rate of spread (such as in the northern heading region in Figs 7*e*, 8*a*), a concave shape such as a canyon was seen to accelerate the fire rate of spread, both through direct effects on that rate and fire–atmosphere feedbacks (as in the southern heading region of Figs 7*e*, 8*a*, *b*).

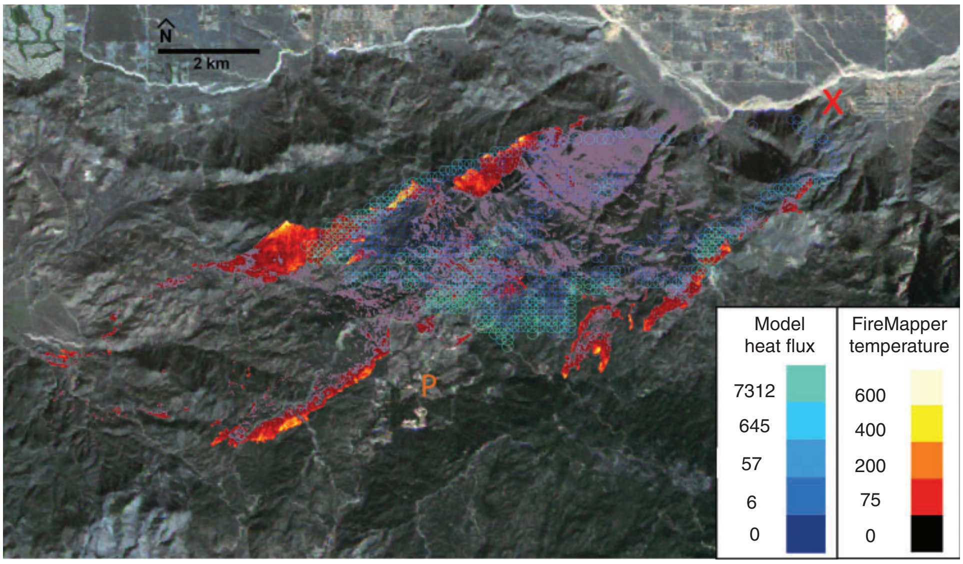

Fig. 10. Overlay of model and map at 1117 hours Pacific Daylight Time. The model sensible heat flux varies from dark blue (lowest) to bright green (highest) as shown in the first colour bar. FireMapper brightness temperature is given by the second colour bar. A red 'X' indicates the ignition location, whereas 'P' indicates Poppet Flats.

Later fire growth and comparison with aircraft observations

At the aircraft's first pass at 1117 hours PDT, the Esperanza Fire's primary run had travelled 16 km west-south-westward from its ignition point, encountering vegetation that was 6–10 years old and that released little energy, as evidenced by low temperatures and narrow flaming zone recorded by the radiometer at the fire's head and the discontinuities across areas of elevated surface temperature (Fig. 9*a*). Substantial regions of high temperature occurred primarily on north-facing aspects and in higher productivity vegetation along the fire's north flank, particularly as the fire ascended the half-pipe walls and in vegetation greater than 50 years old in the south-west. A separate flank run developed to the south-east (Fig. 9*b*). Other isolated runs downwind occurred along the fire's southern flank, such as immediately east of the fire's main head in vegetation older than 50 years.

Comparison of the simulated fire's extent and the first FireMapper image at 1117 hours PDT (Fig. 10) showed that the simulated fire reproduced the rapid spread west-south-westward and agreed with the observed width, shape and splitting of the fire, and general location of the two heading regions. Both FireMapper (Fig. 9*a*, *b*) and the simulation showed fine-scale variation at similar spatial scales along the fire line's leading edge, at which occurred local opportunities for growth that could amplify, producing a feathering effect and flank runs. As the two simulated heading regions expanded, they rejoined, leaving islands of unburned fuel; these occurred between heading regions in FireMapper data as well (Fig. 10), notably around Poppet Flats. In addition, there was general correspondence between regions of high surface temperature, as shown by FireMapper, and modelled high rates of sensible heat flux (e.g. Figs 7*e*, 10).

Spread of the simulated fire slowed after it crested the ridge south-west of Highway 243 (Fig. 11) as the simulated Santa Ana winds weakened prematurely. Although the simulation reproduced the spread over the first 6 h through the time of the fatality, it underestimated the average rate of spread over the subsequent 10 h through this descent – the actual fire had progressed ~16 km in total, whereas the modelled fire had advanced ~11 km. A comparison of simulated airflow with and without feedback from the fire (Fig. 12) showed that fire-induced winds, rather than ambient winds, produced winds in alignment with the drainage. In addition, fire-induced winds produced horizontal roll vortices along the northern heading region and horizontal shear in winds along the southern flank that created counter-clockwise rotation (a 0.8–1.0 km-wide fire whirl). In addition, one of the modelled fire's effects was to draw air upslope towards the north-east in the ridge's lee in the lowest 100 m, against the prevailing flow, to supply air into the fire updrafts. Superimposed on the otherwise relatively weak downslope flow that would have occurred in the ridge's lee without the fire, the net winds were thus insufficient to drive the fire downslope.

The simulation reproduced other features observed by remote sensing. FireMapper showed that at 1117 hours PDT the most intense burning occurred along the fire's northern flank as it climbed the slopes of Mount Edna, coincident with a deep smoke plume (4.7 km above MSL) recorded there by Landsat (Fig. 13). The simulated fire also produced a deep smoke plume from 0940 to 1045 hours PDT, with the height increasing from 3.0 to 4.2 km above MSL as it crossed the slopes of Mount Edna (Fig. 14). By 1117 hours PDT it had crested the mountain and was creeping down the northern slope. The fatality report also noted a deep convective smoke plume rose to between 5.5 and 7.3 km above MSL at 1.6 km south of the fatality site between 0700 and 0800 hours PDT. At 0715 hours PDT in the model, the fire's southern head was 1.8 km south-west of the fatality site and, from 0733 to 0856 hours PDT, produced a deep smoke plume rising to 4.2 km above MSL over the heading region.

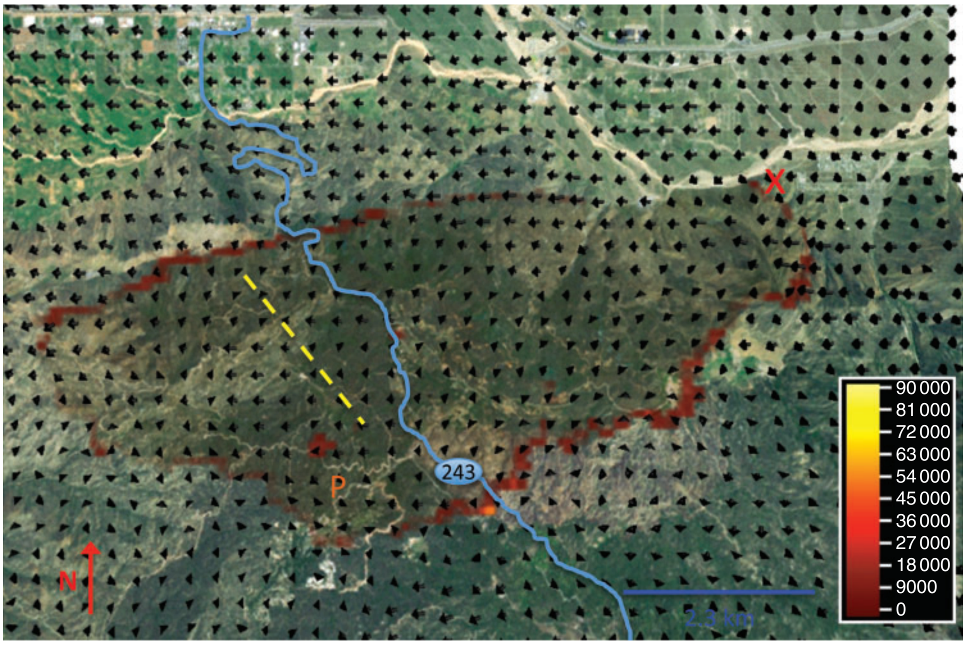

Fig. 11. Modelled fire heat flux (W m^{-2}), and vectors showing the wind every third model grid cell, are shown at 20 m above ground level at 1615 hours Pacific Daylight Time. 'P' indicates Poppet Flats. Ridge 2 (from Fig. 1) shown by dashed yellow line.

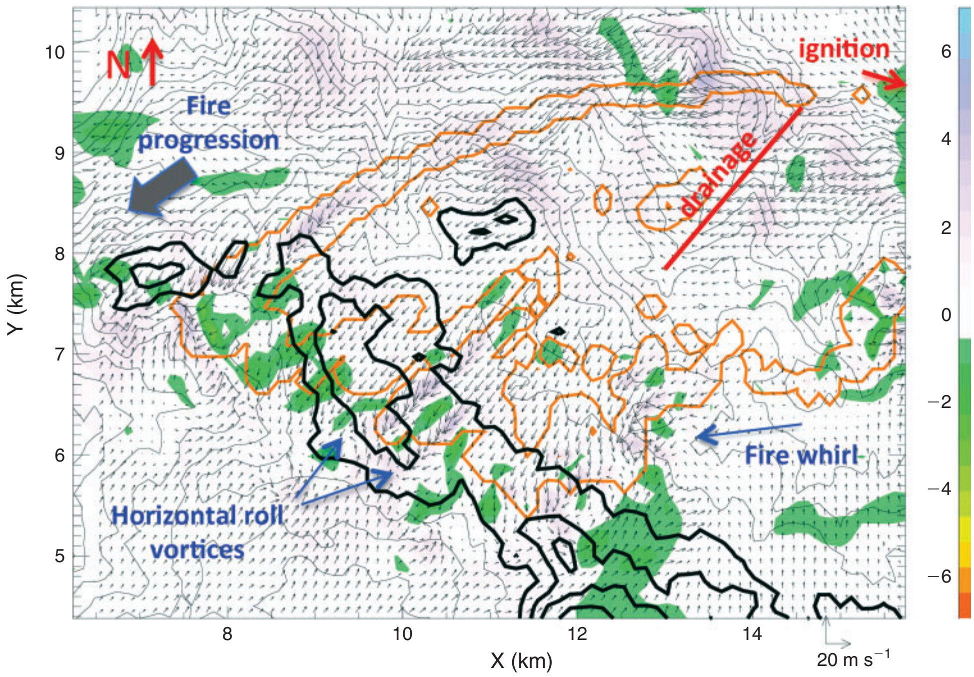

Fig. 12. The difference between a simulation that includes the fire and one without, showing the effect of the fire on the model state (i.e. fire-induced winds) at 1117 hours Pacific Daylight Time at 16 m above ground level. The vectors show the effect of the fire on the horizontal wind components. The colour contours show the effect of the fire on the vertical velocity, coloured according to the colour bar at right. The orange contour contains area where fire's sensible heat flux is >100 W m^{-2}. The ignition location is right of the upper right corner. Black terrain contours are shown every 200 m; the highest four are bold.

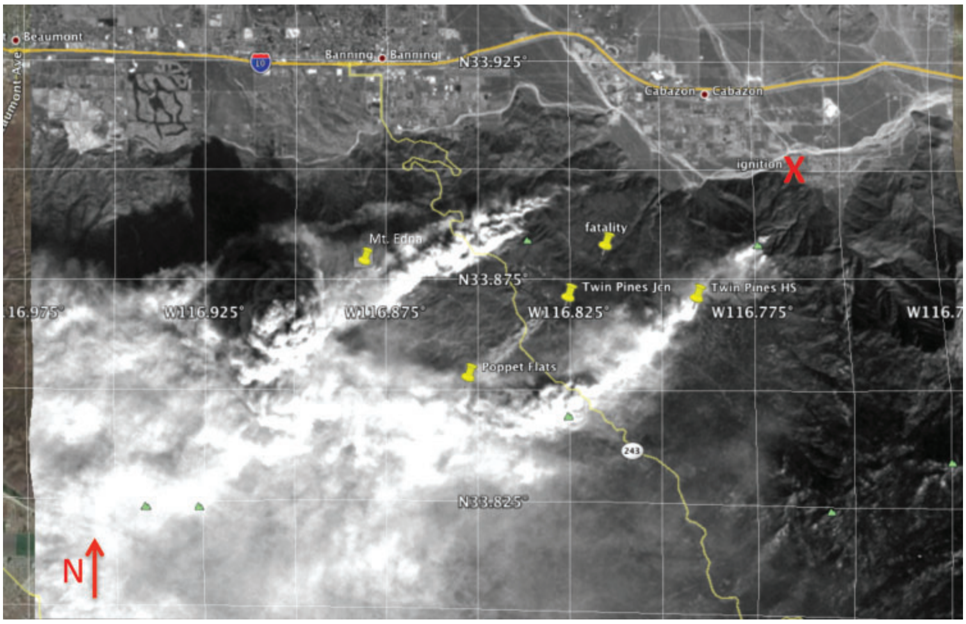

Fig. 13. A Landsat image of smoke at ~1100 hours Pacific Daylight Time showed the burning was occurring primarily around the flanks with a deep plume on the west edge of the north flank near Mount Edna, indicating intense burning.

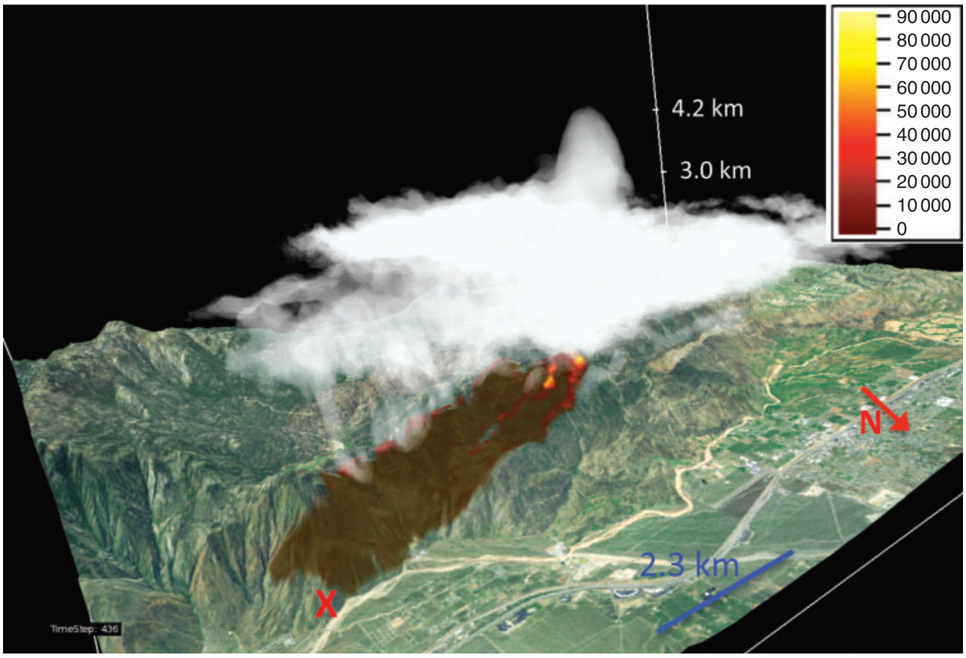

Fig. 14. Smoke (misty white) plumes rose over areas of simulated fire growth on sides of a topographic bowl at 0846 hours Pacific Daylight Time. A red 'X' indicates ignition location.

Sensitivity analyses

In other simulations (not shown), we varied fuel properties including load (doubling it), the fuel particle surface area to volume ratio (σ), and fuel depth; the atmospheric depth over which heat is distributed (α_s); and the distance behind the fire from which wind velocity is used to calculate spread rate. The fire's shape and character were largely unchanged and its extent varied by less than 10%. Of the fuel properties, σ had the greatest effect: casting it towards smaller components, consistent with envisioning fire spread as occurring by piloted contact ignition of small fuel particles, resulted in a flashier fire that spread more readily. With higher average σ, for example, the simulated fire heads spread slightly farther downslope and the shapes of small protuberances were more jagged, although the fire's overall character did not change. We also used fuel loads derived from remote sensing data according to the techniques described in Riggan *et al.* (2010), in which the primary differences were that fuel loads at lower elevations were half or less than the LANDFIRE-derived values but 2–4 times higher than LANDFIRE-derived values at mid-slope in broad areas dominated by shrubs categorised as Fuel Model 4 or 5 (but with no change in fuel depth, thus increasing the fuel packing ratio). The primary effect was to slow the fire in the earlier period, resulting in a fire that reached locations ~0.5 h later.

Discussion

By capturing details of transient airflows and feedbacks from the fire, the CAWFE simulation was able to reproduce many distinguishing features of the Esperanza Fire despite incorporation in the model of semi-empirical components that originated in small-scale laboratory or experimental fires. We found it was essential to capture not just the orographic channelling of winds between mountain ranges, but also transient topographic and thermodynamic enhancements arising from vertical motions of stably stratified air and the modification of complex flow regimes by heat release from the fire. For example, flow accelerations and a hydraulic jump-like flow in Cabazon Peak's lee were simulated to have accelerated the fire down into the topographic drainage that was associated with firefighter fatalities. Diagnostic flow-simulation tools, such as Wind Wizard (Butler *et al.* 2004), could not have described the transient features and atmospheric stratification and thermodynamic effects on winds that characterised the Esperanza Fire. Similarly, key features of the fire could not have been predicted from reliance on data from one or a few local weather stations, nor from description of the Santa Ana as a simple, synoptic flow from high to low pressure. In fact, FARSITE simulations using four sources of wind information (Weise *et al.* 2007), including a RAWS, a meso-scale model, a regional spectral model and the Wind Wizard diagnostic tool, incorrectly described the fire as spreading due west in Banning Pass instead of west-southwestward up into the San Jacinto wilderness. Two factors may explain this discrepancy. First, some topographic flow effects described here were not captured in Weise *et al.*'s two weather model-driven experiments because their horizontal grid spacing was 8–32 times coarser. Second, fire-induced winds (the magnitude of which was comparable to ambient winds) drove the fire up the drainage; Weise *et al.* (2007) did not capture these with their one-way coupling between weather and fire models.

The fire was directed by local winds and the local slope (including both the inclination and concavity of terrain); these combined at different locations and times with either reinforcing or opposing effects on fire spread. This was seen, for instance, where the simulated leading edge of the Esperanza Fire branched into protuberances as it found favourable routes for locally increased growth. Yet we found that when one segment of the fire front found favourable growth downwind while a nearby segment was drawn up canyon, orthogonal to the wind, the fire's leading edge was split into two heading regions. Along a flank, this behaviour led to flanking runs.

Ultimately, the simulation captured the fire's overall direction, width and splitting, and the general shape of lobes on the fire line. The simulated rate of spread across complex but generally inclined terrain (east of Highway 243) was similar to that observed. It also captured intense burning observed on the fire's flanks where the fire experienced local growth as it climbed out of a half-pipe, with creation of strong updrafts and deep smoke plumes over the growth surge. The simulation was less successful in describing the fire spread across a descending landscape later during the first day as the simulated Santa Ana winds had weakened earlier than observed and were too weak to drive the fire downhill against mild upslope winds created by the fire. Note that the overall shape of the simulated fire was neither imposed in the simulation nor subject to elliptical growth imposed at points along the fire line (as in FARSITE), but developed due to dynamic interactions of fire, atmospheric processes and terrain. The coupling produced phenomena such as horizontal roll vortices and rotating updrafts, of which observations were not available.

Simulations varying individual fuel properties such as fuel load (σ) and fuel depth across a range of possible values suggested that their effects were of secondary importance and, in these modelling results, neither altered the event's character nor significantly changed its timing. This concurs with previous modelling studies (Coen *et al.* 2013) and experiments (Cheney *et al.* 1993, Dupuy 1995, McAlpine 1995) that suggested the rate of spread depends weakly or not at all on fuel load. The underlying Rothermel (1972) surface fire spread relationship makes it probable that, were there not strong ambient or fire-induced winds, fuel properties would have a greater effect on the modelled fire's chronology. This relative insensitivity of the event's character to fuel properties does not necessarily apply to fire effects. As experiments in Coen *et al.* (2013) showed, in a coupled model, higher fuel loads led to a stronger, deeper plume, affecting smoke transport and the height of thermal damage to vegetation, but did not strongly affect the fire's rate of spread, although those experiments were limited to flat ground. FireMapper imagery showed that temperatures and energy release in fire fronts, which are important in fire effects, were clearly related to vegetation age and aspect, which are reasonable surrogates for fuel loading.

There are limitations to our approach, namely, the well-recognised limits to predictability, particularly the limits to simulating details of fine-scale features and the deterioration of a weather simulation with time from initialisation. Science gaps hamper the treatment of variables that could be important, for example, quantifying the effect of live fuel moisture on the rate of spread in chaparral, which is not estimated here. It is also extremely difficult to gather complete datasets for input and validation at the scale and resolution of the phenomena. New approaches and datasets for validation must be developed that emphasise remote sensing of fire physical properties. The heat flux and other physical phenomena along a fire line vary greatly, so airborne and high-resolution satellite measurements that can map a fire's spatial variability provide a perspective unmatched by ground-based measurements such as those described in Frankman (2009) that characterise a point on the fire line, if it were even possible to establish instrumentation ahead of a major fire.

Albert Einstein paraphrased Occam's razor, advising that everything should be kept as simple as possible, but no simpler. If the purpose is to rapidly estimate the immediate rate of spread of a simply shaped flaming front or to project the fire perimeter using current conditions without concern for the mechanisms and forces causing this to occur, current operational tools may produce an acceptable result. However, full numerical weather prediction models that capture transient airflow effects and feedbacks from the fire are the minimum required to understand the forces that cause this growth; to capture where fuels, terrain and wind amplify fire growth in blowups; to simulate fire phenomena such as fire whirls or flank runs; or to simulate the unfolding of large fire events with all of their complexity.

Acknowledgements

This material is based upon work supported by the National Science Foundation (NSF) under Grants 0324910, 0421498 and 0835598, and the Federal Emergency Management Agency under Award EMW-2011-FP-01124. The National Center for Atmospheric Research is sponsored by NSF. Any opinions, findings and conclusions or recommendations expressed in this material are the authors' and do not necessarily reflect the views of NSF. We thank Charles Jones, Francis Fujioka, David Weise and Shyh-Chin Chen for their insights. We thank Jeff Zimmerman for photographs, and Lynn Wolden and Robert Tissell for producing images used in this paper. No endorsement by the USDA is implied. Trade names are provided for informational purposes only and do not constitute endorsement by the USDA. Part of the manuscript was prepared by USA government employees on official time and is therefore not subject to copyright and is in the public domain.

References

Albini FA (1976) Estimating wildfire behavior and effects. USDA Forest Service Intermountain Forest and Range Experiment Station, General Technical Report INT-30. (Ogden, UT)

Anderson HE (1982) Aids to determining fuel models for estimating fire behavior. USDA Forest Service, Intermountain Forest and Range Experiment Station, General Technical Report INT-122. (Ogden, UT)

Andrews PL (2009) BehavePlus fire modeling system, version 5.0: Variables. USDA Forest Service, Rocky Mountain Research Station, General Technical Report RMRS-GTR-213WWW Revised. (Fort Collins, CO)

Batchelor GK (1967) 'An Introduction to Fluid Dynamics.' (Cambridge University Press: Cambridge, UK)

Bilgili E, Saglam B (2003) Fire behavior in maquis fuels in Turkey. *Forest Ecology and Management* **184**, 201–207. doi:10.1016/S0378-1127(03)00208-1

Butler BW, Forthofer JM, Finney M, Bradshaw LS, Stratton R (2004) High resolution wind direction and speed information for support of fire operations. In 'Monitoring Science and Technology Symposium: Unifying Knowledge for Sustainability in the Western Hemisphere', 20–24 September 2004, Denver, CO. (Eds C Aguirre-Bravo, PJ Pellicane, DP Burns, S Draggan) USDA Forest Service, Rocky Mountain Research Station, Proceedings RMRS-P-37CD, (Fort Collins, CO) Available at http://www.fs.fed.us/rm/pubs/rmrs_p042.pdf [Verified 14 May 2014]

Cheney NP, Gould JS, Catchpole WR (1993) The influence of fuel, weather and fire shape variables on fire-spread in grasslands. *International Journal of Wildland Fire* **3**, 31–44. doi:10.1071/WF9930031

Cheney NP, Gould JS, Catchpole WR (1998) Prediction of fire spread in grasslands. *International Journal of Wildland Fire* **8**, 1–13. doi:10.1071/WF9980001

Coen JL (2013) Modeling wildland fires: a description of the Coupled Atmosphere–Wildland Fire Environment model (CAWFE). NCAR Technical Note NCAR/TN-500+STR. Available at http://nldr.library.ucar.edu/repository/collections/TECH-NOTE-000-000-000-866 [Verified 13 April 2014]

Coen JL, Schroeder W (2013) Use of spatially refined satellite remote sensing fire detection data to initialize and evaluate coupled weather–wildfire growth model simulations. *Geophysical Research Letters* **40**, 5536–5541. doi:10.1002/2013GL057868

Coen JL, Cameron M, Michalakes J, Patton E, Riggan P, Yedinak K (2013) WRF-Fire: coupled weather–wildland fire modeling with the Weather Research and Forecasting model. *Journal of Applied Meteorology and Climatology* **52**, 16–38. doi:10.1175/JAMC-D-12-023.1

Dennison PE, Moritz MA, Taylor RS (2008) Evaluating predictive models of critical live fuel moisture in the Santa Monica Mountains, California. *International Journal of Wildland Fire* **17**, 18–27. doi:10.1071/WF07017

Dupuy JL (1995) Slope and fuel load effects on fire behavior: laboratory experiments in pine needles fuel beds. *International Journal of Wildland Fire* **5**, 153–164. doi:10.1071/WF9950153

Durran DR (1986) Another look at downslope windstorms. Part I. On the development of analogs to supercritical flow in an infinitely deep, continuously stratified fluid. *Journal of the Atmospheric Sciences* **43**, 2527–2543. doi:10.1175/1520-0469(1986)043<2527:ALADWP>2.0.CO;2

Esperanza Investigation Team (2007) Esperanza Fire accident investigation factual report, Riverside County, CA. Available at http://www.fire.ca.gov/fire_protection/downloads/esperanza_00_complete_final_draft_05_01_2007.pdf [Verified 13 April 2014]

Fernandes PAM (2001) Fire spread prediction in shrub fuels in Portugal. *Forest Ecology and Management* **144**, 67–74. doi:10.1016/S0378-1127(00)00363-7

Fernandes PM, Catchpole WR, Rego FC (2000) Shrubland fire behaviour modelling with microplot data. *Canadian Journal of Forest Research* **30**, 889–899. doi:10.1139/X00-012

Finney MA (1998) FARSITE: Fire Area Simulator – model development and evaluation. USDA Forest Service, Rocky Mountain Station, Research Paper RMRS-RP-4. (Ogden, UT)

Fosberg MA (1965) A case study of the Santa Ana winds in the San Gabriel Mountains. USDA Forest Service, Pacific Southwest Forest and Range Experimental Station, Research Paper PSW-78. (Berkeley, CA)

Fosberg MA, Schroeder MJ (1973) Fine herbaceous fuels in fire-danger rating. USDA Forest Service, Rocky Mountain Forest and Range Experiment Station, Research Note RM-185. (Fort Collins, CO)

Fosberg MA, O'Dell CA, Schroeder MJ (1966) Some characteristics of the three-dimensional structure of Santa Ana winds. USDA Forest Service, Pacific Southwest Forest and Range Experimental Station, Research Paper PSW-30. (Berkeley, CA)

Frankman DJ (2009) Radiation and convection heat transfer in wildland fire environments. PhD thesis, Brigham Young University, Provo, UT.

Haines DA (1982) Horizontal roll vortices and crown fires. *Journal of Applied Meteorology* **21**, 751–763. doi:10.1175/1520-0450(1982)021<0751:HRVACF>2.0.CO;2

Huang C, Lin Y, Kaplan ML, Charney JJ (2009) Synoptic-scale and mesoscale environments conducive to forest fires during the October 2003 extreme fire event in southern California. *Journal of Applied Meteorology and Climatology* **48**, 553–579. doi:10.1175/2008JAMC1818.1

Hughes M, Hall A (2010) Local and synoptic mechanisms causing Southern California's Santa Ana winds. *Climate Dynamics* **34**, 847–857. doi:10.1007/S00382-009-0650-4

Hunt JCR, Feng Y, Linden PF, Greenslade MD, Mobbs SD (1997) Low-Froude-number stable flows past mountains. *Nuovo Cimento-Societa Ocieta Italiana a di Fisica Sezione C* **20**, 261–272.

Lindenmuth AW, Davis JR (1973) Predicting fire spread in Arizona's oak chaparral. USDA Forest Service, Rocky Mountain Forest and Range Experiment Station, Research Paper RM-101. (Fort Collins, CO)

McAlpine RS (1995) Testing the effect of fuel consumption on fire spread rate. *International Journal of Wildland Fire* **5**, 143–152. doi:10.1071/WF9950143

Riggan PJ, Franklin SE, Brass JA, Brooks FE (1994) Perspectives on fire management in Mediterranean ecosystems of southern California. In 'The Role of Fire in Mediterranean-type Ecosystems'. (Eds JM Moreno, WC Oechel) pp. 140–162. (Springer-Verlag: New York)

Riggan PJ, Wolden LG, Tissell RG, Coen J (2010) Remote sensing fire and fuels in southern California. In 'Proceedings of 3rd Fire Behavior and Fuels Conference', 25–29 October 2010, Spokane, Washington. (Ed. D Wade) (CD-ROM) (International Association of Wildland Fire: Birmingham, AL)

Rothermel RC (1972) A mathematical model for predicting fire spread in wildland fuels. USDA Forest Service, Intermountain Forest and Range Experiment Station, Research Paper INT-115. (Ogden, UT)

Ryan BC (1969) A vertical perspective of Santa Ana winds in a canyon. USDA Forest Service, Pacific Southwest Forest and Range Experimental Station, Research Paper PSW-52. (Berkeley, CA)

Schroeder MJ, Glovinsky M, Henricks VF, Hood FC, Hull MK (1964) Synoptic weather types associated with critical fire weather. USDA Forest Service, Pacific Southwest Forest and Range Experiment Station, report 0036944. (Berkeley, CA)

Stephens SL, Weise DR, Fry DL, Keiffer RJ, Dawson J, Koo E, Potts J, Pagni PJ (2008) Measuring the rate of spread of chaparral prescribed fires in northern California. *Fire Ecology* **4**, 74–86. doi:10.4996/FIRECOLOGY.0401074

Vosper SB, Castro IP, Snyder WH, Mobbs SD (1999) Experimental studies of strongly stratified flow past three-dimensional orography. *Journal of Fluid Mechanics* **390**, 223–249. doi:10.1017/S0022112099005133

Weise DR, Zhou X, Sun L, Mahalingam S (2005) Fire spread in chaparral -'go or no-go?' *International Journal of Wildland Fire* **14**, 99–106. doi:10.1071/WF04049

Weise DR, Chen S, Riggan PJ, Fujioka FM (2007) Using high-resolution weather data to predict fire spread using the FARSITE simulator – a case study in southern California chaparral. In 'Proceedings of the Seventh Symposium on Fire and Forest Meteorology', 23–25 October 2007, Bar Harbor, ME. Paper 8.2. (American Meteorological Society: Boston, MA, USA) Available at https://ams.confex.com/ams/pdfpapers/126873.pdf [Verified 13 April 2014]

Whiteman CD (2000) 'Mountain Meteorology: Fundamentals and Applications.' (Oxford University Press: New York)